

Enhanced charge recombination due to surfaces and twin defects in GaAs nanostructures

Evan Brown, Chunyang Sheng, Kohei Shimamura, Fuyuki Shimojo, and Aiichiro Nakano

Citation: [Journal of Applied Physics](#) **117**, 054307 (2015); doi: 10.1063/1.4907534

View online: <http://dx.doi.org/10.1063/1.4907534>

View Table of Contents: <http://scitation.aip.org/content/aip/journal/jap/117/5?ver=pdfcov>

Published by the [AIP Publishing](#)

Articles you may be interested in

[Twin superlattice-induced large surface recombination velocity in GaAs nanostructures](#)

Appl. Phys. Lett. **105**, 231602 (2014); 10.1063/1.4903487

[Effects of twins on the electronic properties of GaAs](#)

Appl. Phys. Lett. **103**, 022105 (2013); 10.1063/1.4811746

[Photovoltaic effects on Franz–Keldysh oscillations in photoreflectance spectra: Application to determination of surface Fermi level and surface recombination velocity in undoped GaAs/n-type GaAs epitaxial layer structures](#)

J. Appl. Phys. **97**, 063708 (2005); 10.1063/1.1861968

[Surface and bulk passivation of GaAs solar cell on Si substrate by H₂ + PH₃ plasma](#)

Appl. Phys. Lett. **76**, 730 (2000); 10.1063/1.125876

[Detection of surface states in GaAs and InP by thermally stimulated exoelectron emission spectroscopy](#)

J. Appl. Phys. **82**, 5597 (1997); 10.1063/1.366420

A promotional banner for the Journal of Applied Physics. It features the AIP logo and the journal title at the top. Below that, the text 'Meet The New Deputy Editors' is displayed. Three circular headshots of the new deputy editors are shown: Christian Brosseau, Laurie McNeil, and Simon Phillpot, each with their name written below their photo.

AIP | Journal of Applied Physics

Meet The New Deputy Editors

 Christian Brosseau

 Laurie McNeil

 Simon Phillpot

Enhanced charge recombination due to surfaces and twin defects in GaAs nanostructures

Evan Brown,¹ Chunyang Sheng,¹ Kohei Shimamura,^{1,2} Fuyuki Shimojo,^{1,2} and Aiichiro Nakano¹

¹*Collaboratory for Advanced Computing and Simulations, Department of Physics & Astronomy, Department of Computer Science, Department of Chemical Engineering & Materials Science, University of Southern California, Los Angeles, California 90089-0242, USA*

²*Department of Physics, Kumamoto University, Kumamoto 860-8555, Japan*

(Received 6 December 2014; accepted 22 January 2015; published online 4 February 2015)

Power conversion efficiency of gallium arsenide (GaAs) nanowire (NW) solar cells is severely limited by enhanced charge recombination (CR) at sidewall surfaces, but its atomistic mechanisms are not well understood. In addition, GaAs NWs usually contain a high density of twin defects that form a twin superlattice, but its effects on CR dynamics are largely unknown. Here, quantum molecular dynamics (QMD) simulations reveal the existence of an intrinsic type-II heterostructure at the (110) GaAs surface. Nonadiabatic quantum molecular dynamics (NAQMD) simulations show that the resulting staggered band alignment causes a photoexcited electron in the bulk to rapidly transfer to the surface. We have found orders-of-magnitude enhancement of the CR rate at the surface compared with the bulk value. Furthermore, QMD and NAQMD simulations show unique surface electronic states at alternating (111)A and (111)B sidewall surfaces of a twinned [111]-oriented GaAs NW, which act as effective CR centers. The calculated large surface recombination velocity quantitatively explains recent experimental observations and provides microscopic understanding of the underlying CR processes. © 2015 AIP Publishing LLC. [<http://dx.doi.org/10.1063/1.4907534>]

I. INTRODUCTION

Semiconductor nanowires (NWs) are used in many devices, such as solar cells.¹ Gallium arsenide (GaAs) is one of the most widely studied semiconductors for NW applications. Despite impressive recent progress,^{2–4} however, GaAs NW solar cells still suffer low power conversion efficiency. The low efficiency is generally attributed to the large charge-recombination (CR) rate at NW sidewall surfaces. Namely, a large fraction of photoexcited electron-hole pairs recombine and are lost before they are collected as an electric current. In fact, optical pump-terahertz probe time domain spectroscopy has shown orders-of-magnitude higher surface CR rates for GaAs NWs compared with those in InAs and InP.⁵ However, the atomistic mechanisms underlying the observed high surface CR rate in GaAs remain elusive.

A typical [111]-oriented GaAs NW has a hexagonal cross section with six sidewall facets that are nominally {110} lattice planes. Among many unique features, these semiconductor NWs usually contain a high density of twin defects that form a twin superlattice (TSL).^{6–8} The geometry of TSLs has been studied extensively. In a [111]-oriented III–V semiconductor NW with a hexagonal cross section, a TSL is commonly accompanied by alternating (111)A and (111)B sidewall surfaces^{6–8} instead of {110} sidewalls. These TSLs greatly affect the electronic properties of NWs. For example, they surprisingly increase the radiative decay time of a bound exciton while decreasing the carrier mobility in a [111] oriented GaAs NW.^{9,10} However, the effect of ubiquitous TSLs on the CR rate remains elusive. Thus, key scientific questions are (1) how is the electronic structure of GaAs modified at different crystallographic surfaces, and

how is the CR rate affected by the modification, and (2) what is the effect of TSLs on surface electronic states, and how do they influence CR dynamics in GaAs NWs?

To answer these questions, we first perform quantum molecular dynamics (QMD) simulations,^{11–15} which follow the trajectories of all atoms while computing interatomic forces from first-principles based density functional theory (DFT).^{16,17} Simulation results reveal the existence of an intrinsic type-II (or staggered) heterostructure at the (110) GaAs surface. Subsequently, we perform nonadiabatic quantum molecular dynamics (NAQMD) simulations^{18–22} to study photoexcitation dynamics in this system. Simulation results show that the staggered band alignment causes a photoexcited electron in the bulk to rapidly transfer to the surface. We have found orders-of-magnitude enhancement of the CR rate at the surface compared with the bulk value. Nevertheless, the calculated CR rate at the (110) surface is orders-of-magnitude smaller than experimentally inferred values.⁵

To identify the cause of this discrepancy, we next perform QMD and NAQMD simulations of alternating (111)A and (111)B sidewall surfaces in a twinned [111]-oriented GaAs NW. Simulation results show unique surface electronic states at the alternating (111)A and (111)B surfaces, which act as effective CR centers. The calculated large CR rates and the associated surface recombination velocity (SRV) quantitatively explain recent experimental observations.⁵

II. SIMULATION METHODS

A. Quantum molecular dynamics

We study the electronic structures at surfaces using QMD simulations.^{11–15} Here, electronic states are calculated

using the projector-augmented-wave method,^{23,24} which is an all-electron electronic-structure-calculation method within a frozen-core approximation. The generalized gradient approximation²⁵ is used for the exchange-correlation energy with nonlinear core corrections.²⁶ We apply self-interaction corrections to the energies of the Kohn-Sham (KS) orbitals.^{27,28} The momentum-space formalism is utilized,²⁹ where the plane-wave cutoff energies are 30 and 250 Ry for the electronic pseudo-wave functions and the pseudo-charge density, respectively. The energy is minimized with respect to the KS orbitals iteratively using a preconditioned conjugate-gradient method. Projector functions are generated for the 4s, 4p, and 4d states of Ga and As. We use our own QMD code, which has been implemented on parallel computers by a hybrid approach combining spatial decomposition (i.e., distributing real-space or reciprocal-space grid points among processors) and band decomposition (i.e., assigning the calculations of different KS wave functions to different processors).^{30,31} The program is written using the message passing interface (MPI) library³² for interprocessor communications.

B. Nonadiabatic quantum molecular dynamics

To study how the surface electronic states affect CR dynamics, we perform NAQMD simulations.^{18–22} The NAQMD method describes electronic excitations in the framework of linear-response time-dependent density functional theory.³³ In addition, nonadiabatic transitions between excited electronic states assisted by molecular motions are treated with a surface-hopping approach.^{34–38} To perform large NAQMD simulations involving many hundreds of atoms, we have implemented a series of techniques for efficiently calculating the long-range exact exchange correction and excited-state forces.^{27,28} Due to the use of excited-state forces, photoexcitation also modifies ground-state electronic structures.

C. System setup

We study two different systems: (1) a (110) surface that corresponds to a sidewall of a hexagonal [111]-oriented GaAs NW and (2) alternating (111)A and (111)B surfaces in a GaAs NW with a TSL.

To study a (110) surface, a slab of $19.58 \times 20.77 \times 18.25 \text{ \AA}^3$ containing 180 Ga and 180 As atoms is cut out from the bulk GaAs zinc-blende crystal, where the x , y , and z axes are aligned with the $[\bar{1}11]$, $[1\bar{1}\bar{2}]$, and $[110]$ crystallographic orientations, respectively (Fig. 1(a)). A vacuum layer of thickness 21.74 \AA is added in the z direction, thereby exposing two $\{110\}$ surfaces. The dangling bonds on the bottom surface are terminated by hydrogen atoms, whereas the top surface is not passivated. Periodic boundary conditions (PBCs) are applied to all Cartesian directions for the resulting simulation supercell of dimensions $19.58 \times 20.77 \times 39.99 \text{ \AA}^3$. The simulated system contains 396 atoms, and the Γ point is used for Brillouin zone sampling. We obtain the minimum-energy atomic configuration by relaxing the atomic positions using the quasi-Newton method. The snapshot of the relaxed configuration in Fig. 1(a) shows considerable upward displacements of As atoms away from the bulk.

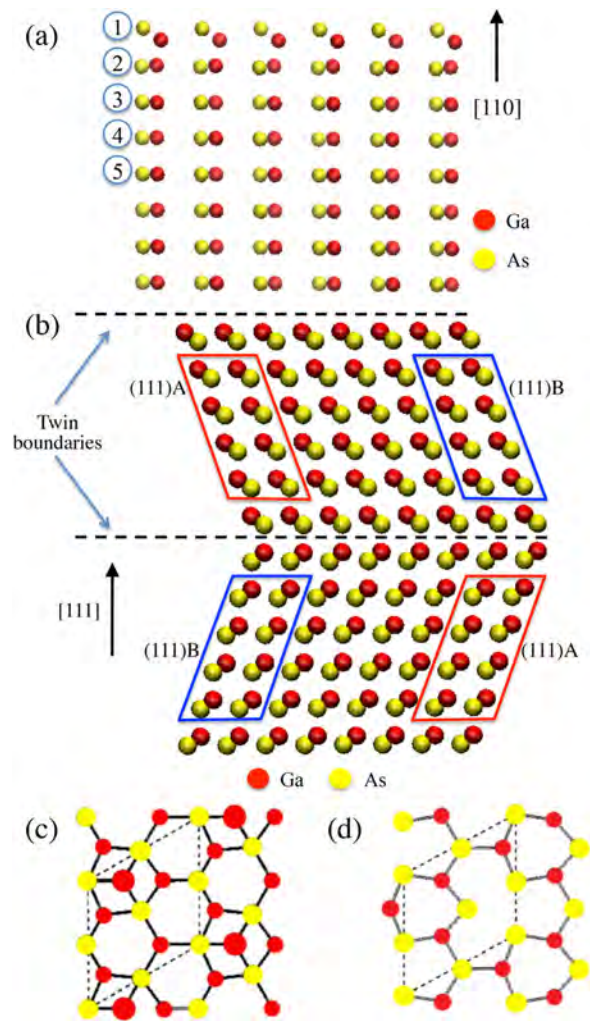


FIG. 1. (a) Relaxed GaAs crystal with a (110) surface on the top viewed from the $[1\bar{1}\bar{2}]$ direction, where red and yellow spheres represent Ga and As atoms, respectively. Atomic bilayers are numbered sequentially starting from that on the (110) surface. (b) Relaxed twinned GaAs nanosheet viewed from the $[1\bar{1}\bar{2}]$ direction. Atoms that belong to (111)A and (111)B regions are enclosed by red and blue lines, respectively. (c) Top view of the Ga-atom reconstruction of GaAs (111)B surface. (d) Top view of the Ga-vacancy reconstruction of (111)A surface.

Next, we consider a twinned GaAs NW. As explained in Sec. I, TSLs in [111]-oriented III-V semiconductor NWs are commonly associated with $\{111\}$ sidewall facets.^{6–8} To simplify the geometry while retaining this key feature, we here simulate a GaAs nanosheet (NS)^{39,40} as shown in Fig. 1(b). The xy -cross section (which is parallel to the (111) crystallographic plane of GaAs zinc blende crystal) of the NS has side lengths of 45.00 \AA and 15.99 \AA in the x and y directions, which are aligned with the $[110]$ and $[11\bar{2}]$ directions, respectively. (111) GaAs bilayers are stacked in such a way as to expose Ga-terminated (111)A and As-terminated (111)B type sidewall surfaces, whereas the PBC is applied in the y direction to emulate an infinite NS. A stacking defect is inserted in the middle of the simulation box in the z direction to revert the stacking sequence (Fig. 1(b)). We apply the PBC in the z direction, and consequently there are two twin boundary planes, one at $z = L_z/2$ and the other at $z = L_z$ or equivalently at $z = 0$ due to the PBC, where $L_z = 39.17 \text{ \AA}$ is

the height of the simulation box in the z direction. This amounts to a TSL with a twin-twin distance of $L_z/2 = 19.58 \text{ \AA}$, which is typical in experimental systems.⁴¹ The simulated system contains 768 atoms, and the Γ point is used for Brillouin zone sampling.

For the twinned GaAs, we obtain the minimum-energy atomic configuration by relaxing the atomic positions using the quasi-Newton method. By doing so with ideal (111)A and (111)B sidewall surfaces, we found the configuration to be mechanically unstable, with some Ga atoms detaching from the (111)A surfaces. This instability is understandable in light of the relatively high surface energies of the ideal surfaces compared to some of the reconstructed surfaces.⁴² We thus consider GaAs (111)B sidewalls with Ga-atom reconstructions (Fig. 1(c)) and GaAs (111)A sidewalls with Ga-vacancy reconstructions (Fig. 1(d)). These reconstructed surfaces are charge-neutral and have the lowest surface energies compared with other surfaces at most Ga and As vapor pressures.⁴² The NS with these reconstructed sidewall surfaces remains stable during the quasi-Newton energy minimization.

III. RESULTS FOR A (110) SURFACE

A. Surface electronic states

We study the bending of energy bands near the GaAs (110) surface. This can be done by calculating the electronic partial density-of-states²² (PDOS) $D_n(E)$ projected onto the wave functions of the atoms in the n -th (110) atomic bilayer along the z axis. Numbering of bilayers is defined in Fig. 1(a). In Fig. 2, the red curves show the calculated $D_n(E)$, where the origin of the energy is the Fermi energy. As we move away from the surface, the PDOS quickly converges to the bulk behavior (see the curves in bilayer 3–5), where the band gap takes the bulk value of 1.5 eV. The left and right blue lines in Fig. 2 denote the valence-band (VB) and conduction-band (CB) edges, respectively.²⁷ In contrast, the PDOS in the two top bilayers near the (110) surface exhibit

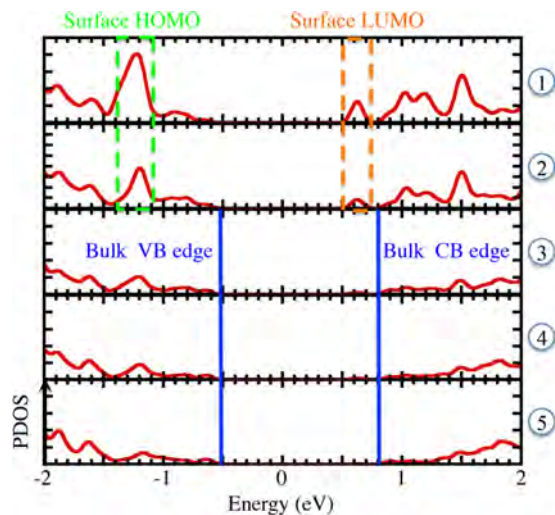


FIG. 2. Intrinsic type-II heterostructure at the GaAs (110) surface. Electronic PDOS projected onto the atomic bilayers defined in Fig. 1(a) are shown by red curves. Bulk CB and VB edge energies are marked by blue lines. The LUMO and HOMO at the surface are marked by orange and green dashed boxes, respectively.

markedly different behaviors. In both bilayers 1 and 2, there is a peak around 0.6 eV slightly below the bulk CB edge. This peak corresponds to the lowest unoccupied molecular orbital (LUMO) on the surface. The surface PDOS in bilayers 1 and 2 has another peak around -1.3 eV, which is below the bulk VB edge. This peak corresponds to the highest occupied molecular orbital (HOMO) on the surface. Namely, the surface LUMO and HOMO exhibit a staggered band alignment with the bulk CB-VB edges. In other words, surface relaxation causes the spontaneous formation of an intrinsic type-II heterostructure (as opposed to ordinary heterostructures made by dissimilar materials). A similar band alignment for a relaxed GaAs (110) surface was obtained using the GW approximation.⁴³ This intrinsic heterostructure is akin to the formation of intrinsic core-shell structures due to surface relaxation in GaAs (Refs. 10 and 44) and ZnO (Ref. 45) NWs.

To characterize the spatial distribution of the i -th KS wave function $\psi_i(\mathbf{r})$, we calculate its existence probability at the surface

$$P_i = \int_{\mathbf{r} \in \text{surface}} d\mathbf{r} |\psi_i(\mathbf{r})|^2,$$

where the surface region is defined as the top two bilayers. Figure 3 plots P_i as a function of the KS energy ε_i . As expected, the LUMOs of the total system around 0.6 eV are largely surface states. On the other hand, the HOMOs around -0.4 eV reside in the bulk. These observations are consistent with the intrinsic type-II heterostructure mentioned above.

B. Charge-recombination dynamics

We consider two types of excitations by exciting one electron from an occupied orbital to an unoccupied orbital. In the first excitation, an electron in the HOMO of the total system is excited to the LUMO of the total system. Note that the LUMO of the total system is a surface state (see Fig. 2), which has a high surface probability over 0.6 (Fig. 3). The second is a bulk excitation (Fig. 2), where an electron is

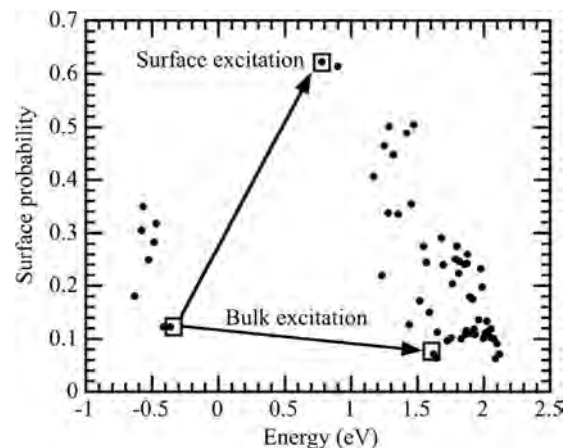


FIG. 3. Existence probability of KS wave functions at the surface as a function of the KS energy. Bulk- and surface-excitation simulations are initiated by the transitions denoted by arrows.

excited from the HOMO of the total system to an orbital with a very small surface probability less than 0.1 (Fig. 3).

In the NAQMD simulation for the bulk excitation, the excited electron quickly transfers to the surface. Figure 4 shows snapshots of the electron and hole wave functions at times 0 and 169 fs. In Fig. 4(a) at time 0, both the electron and hole wave functions spread across the entire system. In contrast, the electron has largely transferred to the surface region by 169 fs, while the hole remains in the bulk (Fig. 4(b)), which is expected from the intrinsic type-II heterostructure. The staggered band alignment drives a photoexcited electron in the bulk to lower energy surface states, whereas holes remain near the VB edge (which is a bulk state). The charge-transfer (CT) from the bulk to the surface is assisted by thermal molecular motions.^{22,46} From the time evolution of the surface probability of the excited electron, we estimate the CT rate to be $k_{CT} = 6.25 \times 10^{12} \text{ s}^{-1}$.

The NAQMD simulations calculate the transition probability $\gamma_{ij}(t)$ from the current excited state i to another state j as a function of time t . The phonon-assisted CR rate is then estimated as $k_{CR} = \gamma_{ij}(t)/t$, respectively, where i and j are the electron and hole states.^{22,47} Figures 5(a) and 5(b) show the accumulated CR probability $\gamma_{ij}(t)$ from the electron to hole states as a function of time in the bulk- and surface-excitation simulations, respectively. Note that, for the bulk excitation, the time is limited to earlier stages before CT occurs from the bulk to the surface region. From the linear fitting in Fig. 5, the phonon-assisted CR rate is estimated to be $k_{CR\text{-phonon}}^{\text{bulk}} = (1.7 \pm 0.1) \times 10^6 \text{ s}^{-1}$ and $k_{CR\text{-phonon}}^{\text{surface}} = (1.8 \pm 0.1) \times 10^7 \text{ s}^{-1}$ for the bulk- and surface-excitations, respectively. Namely, the CR rate is enhanced by an order-of-magnitude near the surface. This is consistent with the observed large CR rates at GaAs NW sidewall surfaces.⁵ In addition to the phonon-assisted contribution to the CR rate computed by NAQMD, we also estimate the spontaneous emission contribution calculated using the transition dipole approximation.^{21,48} The calculated values, $k_{CR\text{-SE}}^{\text{bulk}} = 2.8 \times 10^2 \text{ s}^{-1}$ and $k_{CR\text{-SE}}^{\text{surface}} = 9.3 \times 10^3 \text{ s}^{-1}$, are far smaller than the corresponding phonon-assisted contributions. Therefore, the latter is the dominant contribution to the CR rate.

Here, it should be noted that the enhanced surface CR rate shown above is still not large enough to explain the

experimentally observed large surface recombination velocities in GaAs NWs.⁵ Potential sources of this discrepancy include the formation of surface oxides⁴⁹ and associated interfacial charge recombination,⁵⁰ as well as other surface defects. Another cause could be the large number of twin defects observed in experimental NWs^{9,10,51} and associated {111} sidewall facets.^{8,51,52} These facets are characterized by surface reconstructions and associated atomic defects, such as vacancies and adatoms,⁴² which likely act as CR hot spots. In Sec. IV, we study CR processes near GaAs {111} surfaces with twin defects.

IV. RESULTS FOR (111) SURFACES AND TWINS

A. Surface electronic states

We study the KS energy levels that lie in the bulk band gap. Since the effect of twin boundaries on the energy levels is known to be very small,^{9,10} such gap states, if they exist, are expected to arise from the resulting alternating (111)A and (111)B sidewall surfaces. To quantify these surface states, we calculate the electronic PDOS (Ref. 22) $D_{\alpha}(E)$ projected onto the wave functions of the atoms in the surface regions ($\alpha = (111)A$ or $(111)B$). The definition of these surface regions is shown in Fig. 1(b). In Fig. 6, the red and blue curves show the calculated $D_{(111)A}(E)$ and $D_{(111)B}(E)$, respectively, where the origin of the energy is the Fermi energy. To show the alignment of these surface energy levels relative to the band gap ($\sim 1.5 \text{ eV}$) of the bulk GaAs, bulk CB and VB energies are marked by orange and green boxes, respectively, in Fig. 6. The gap states derived from (111)A surfaces are located just above the bulk VB top. On the other hand, those derived from (111)B surfaces are located just below the bulk CB bottom. These band alignments are illustrated in Fig. 7.

To understand the nature of the band alignment, we project the CB-edge and VB-edge wave functions onto the pseudoatomic orbitals centered at Ga and As atoms.⁵³ For the CB-edge wave function, 67.6% and 32.4% of the total population come from Ga 4s and As 4s states, respectively.⁹ The partial populations of the three degenerate VB-edge wave functions, on the other hand, are nearly identical: 80.3% and 11.6%, respectively, from As 4p and Ga 4p states.⁹ Namely, the CB wave function is s-like and is centered at Ga atoms,

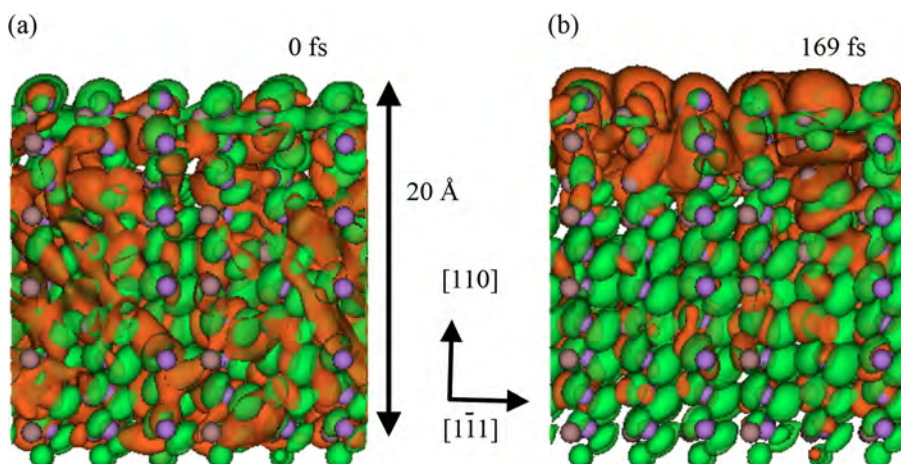


FIG. 4. Electron (orange) and hole (green) wave functions of the bulk-excitation simulation at time 0 and 169 fs.

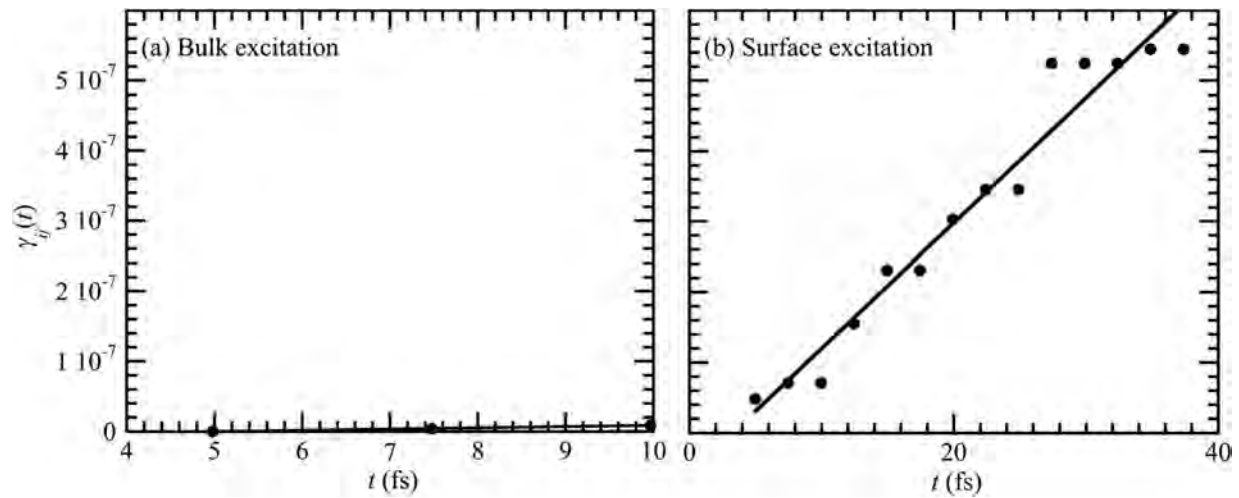


FIG. 5. Accumulated CR probability as a function of time during NAQMD simulations for (a) bulk excitation and (b) surface excitation. The lines show linear fitting.

whereas the VB wave functions are p-like around As atoms. The reconstructed (111)A surface is characterized by Ga vacancy sites, and hence, it is more As-like. Since the VB-edge wave functions reside dominantly on As atoms, it is understandable that the calculated PDOS of (111)A surfaces has a larger weight near the VB edge. On the contrary, the reconstructed (111)B surface has Ga adatoms, and hence is more Ga-like. Accordingly, its PDOS has more weight near the CB edge, where wave functions reside more on Ga atoms.

B. Energy relaxation dynamics of photoexcited electron-hole pairs

To study how the surface gap states affect CR, we perform NAQMD simulations.^{18–22} To mimic photoexcitation in the bulk, we excite an electron from an occupied KS orbital with energy equal to the bulk VB top (Fig. 6) to an unoccupied KS orbital with energy equal to the bulk CB bottom (Fig. 6). In Fig. 8, the blue and red dots show the energy levels of the electron and hole states, respectively, as a function of time. Initially, only one electron-hole pair exists,

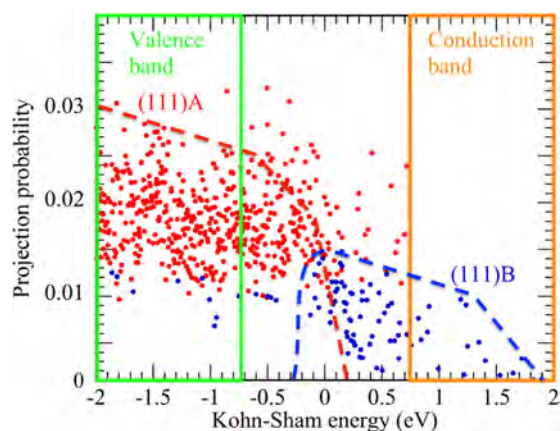


FIG. 6. Surface electronic states. Electronic PDOS projected onto the (111)A and (111)B sidewall surfaces defined in Fig. 1(b) are shown by red and blue curves, respectively. Bulk CB and VB energies are marked by orange and green boxes, respectively.

where the difference between the electron and hole energies is ~ 1.5 eV. Due to nonadiabatic transitions assisted by atomic motions, however, more electron-hole pairs are created starting at ~ 80 fs concentrated near the Fermi energy.

To quantify the CR rate governed by the multiple excitations, we calculate the average electronic excitation energy

$$E_{\text{exc}}(t) = \frac{\sum_i n_i(t) \varepsilon_i(t) \Theta(\varepsilon_i(t)) - \sum_i (2 - n_i(t)) \varepsilon_i(t) \Theta(-\varepsilon_i(t))}{\sum_i n_i(t) \Theta(\varepsilon_i(t)) + \sum_i (2 - n_i(t)) \Theta(-\varepsilon_i(t))}, \quad (1)$$

where $n_i(t)$ and $\varepsilon_i(t)$ are the occupation number and energy of the i -th state at time t , and the step function $\Theta(x)$ is 1 ($x \geq 0$) or 0 ($x < 0$). Figure 9 shows the calculated $E_{\text{exc}}(t)$ in a semi-log plot. The linear decrease represented by the solid line in Fig. 9 indicates an exponential decay of the excitation energy, $E_{\text{exc}}(t) = E_0 \exp(-k_{\text{CR}}t)$, where E_0 is the photoexcitation energy and k_{CR} is the CR rate. The best fit yields $k_{\text{CR}} = (3.0 \pm 0.2) \times 10^{11}$ (s^{-1}). The corresponding decay

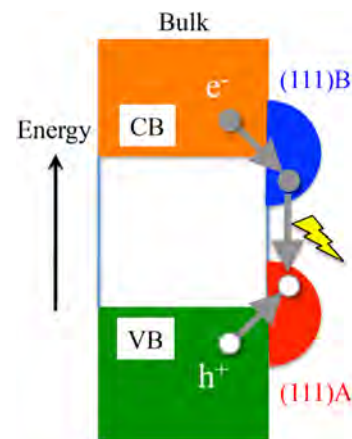


FIG. 7. Schematic of the bulk CB (orange) and VB (green) along with (111)A (red) and (111)B (blue) surface-state energies. Electrons in the bulk CB transfer to the (111)B surface states, where they recombine with holes transferred from the bulk VB to the (111)A surface states.

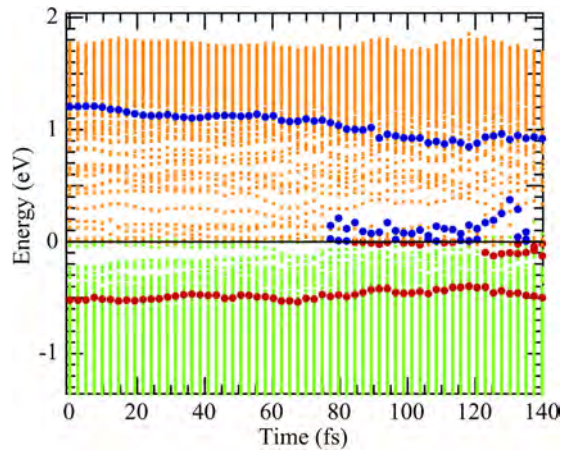


FIG. 8. Energy relaxation of photoexcited electron-hole pairs. Electron (solid blue circle) and hole (solid red circle) energy levels are shown as a function of time. The other occupied and unoccupied energy levels are shown by green and orange dots, respectively.

time of a few ps is consistent with a value inferred for GaAs NWs from recent optical pump-terahertz probe measurements.⁵

C. Surface recombination velocity

The CR time τ in NWs is commonly expressed as

$$\frac{1}{\tau} = \frac{1}{\tau_{\text{bulk}}} + \frac{4S}{d}, \quad (2)$$

where τ_{bulk} is the bulk CR time, d is the NW diameter, and S is the SRV. Joyce *et al.* performed optical pump-terahertz probe experiments to measure the decay time of photoexcited carriers in GaAs NWs of diameter $d=30, 50,$ and 80 nm.⁵ They fitted the measured diameter-dependent decay time to Eq. (2) and estimated $S=5.4 \times 10^3$ m/s.

To compare our NAQMD simulation results with these experiments, we construct a simple model as follows: Consider a cylindrical NW of diameter d , in which the CR rate is much larger than the bulk value in the outer shell of thickness δ as shown in Fig. 10. An electron-hole pair photoexcited in the core of the NW must first diffuse to the shell

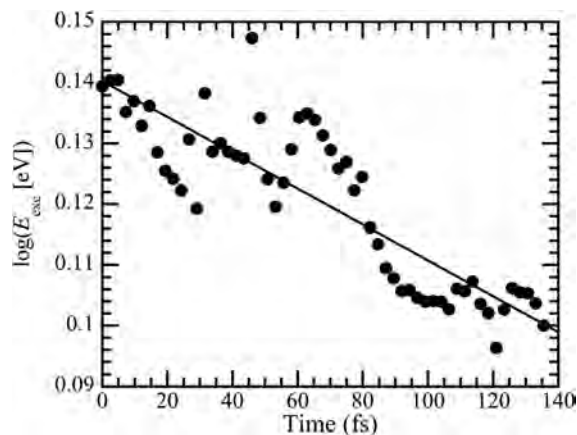


FIG. 9. The average electronic excitation energy as a function of time.

to recombine at a rate of k_{CR} . We solve a simple diffusion-reaction equation for the photoexcited carrier population using the diffusion coefficient of $D=10^{-3}$ m²/s (a typical value for a hole in bulk GaAs). From the spatial decay of typical surface states observed in our simulation, we estimate $\delta=1$ nm.

Figure 11(a) shows the calculated carrier population as a function of time for $d=30, 50,$ and 80 nm. We see more rapid decay of carriers for smaller d . From the exponential fit (solid lines in Fig. 11(a)), we obtain the effective CR rate for each diameter d . Figure 11(b) shows the fitted k_{CR} as a function of d . By fitting the result with Eq. (2), we obtain the SRV to be $(3.6 \pm 0.9) \times 10^3$ m/s. This value is the same order-of-magnitude as the experimental value of 5.4×10^3 m/s. Thus, the TSL and associated $\{111\}$ sidewall surfaces can quantitatively account for the experimentally observed large SRV in GaAs NWs. It is also understandable that the calculated SRV is slightly smaller than the experimental value, since the former is for the ideal reconstructed surfaces and does not include the contributions of surface oxidation and other defects. Possible defects in experimental systems include vacancies and impurities (e.g., carbon) introduced during the growth. Other potential causes of the large SRV include the formation of surface oxides⁴⁹ and associated interfacial CR as mentioned before.⁵⁰

The high SRV of a twinned GaAs NW may be understood as a consequence of the unique electronic structures associated with its geometry (Fig. 7). Namely, alternating (111)A and (111)B sidewall surfaces with, respectively, near VB-edge and CB-edge energies provides spatially proximate CR sites. Photoexcited electrons tend to migrate quickly to (111)B surfaces driven by the energy alignment, while holes migrate to (111)A surfaces. With a high density of twin defects (i.e., short length scales of alternating (111)A and (111)B surface segments as shown in Fig. 1(b)), the electron and hole wave functions have considerable overlap and hence a large CR rate and SRV (Fig. 7). To confirm that the very large SRV is a consequence of the unique surface geometry associated with TSLs, Table I compares the calculated CR rate for alternating (111)A/(111)B sidewall surface in this section with that for a (110) sidewall in Sec. III. The

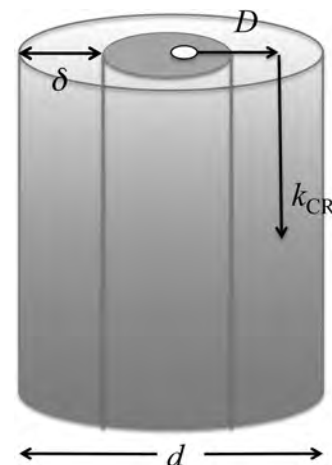


FIG. 10. Schematic of carrier diffusion and CR in a GaAs NW.

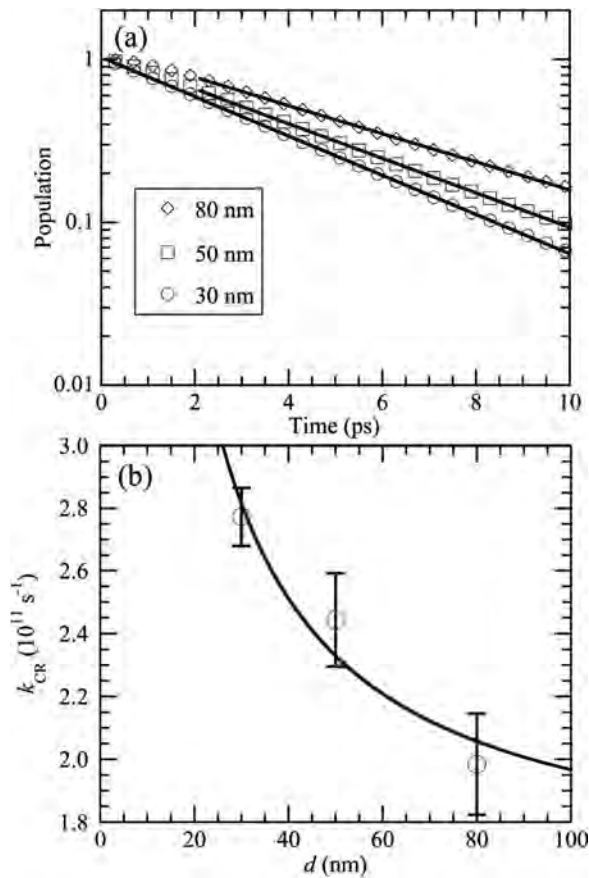


FIG. 11. (a) Carrier population as a function of time for diameter $d = 30, 50,$ and 80 nm . (b) The CR rate as a function of the NW diameter.

TABLE I. The CR rates at (110) and twinned (111) surfaces in GaAs.

	(110)	(111)
$k_{CR} (\text{s}^{-1})$	$(1.8 \pm 0.1) \times 10^7$	$(3.0 \pm 0.2) \times 10^{11}$

k_{CR} at the (110) surface is orders-of-magnitude smaller ($\sim 10^7 \text{ s}^{-1}$). Hence, the much larger CR rate ($\sim 10^{11} \text{ s}^{-1}$) in this section is likely due to the TSL-related surface geometry.

V. CONCLUSION

In summary, our QMD simulations have shown the existence of an intrinsic type-II heterostructure at a (110) GaAs surface. According to our NAQMD simulations, the resulting staggered band alignment causes a photoexcited electron in the bulk to rapidly transfer to the surface. We have found orders-of-magnitude enhancement of the CR rate at the surface compared with the bulk value. Furthermore, our QMD and NAQMD simulations have shown that unique surface electronic states at alternating (111)A and (111)B sidewall surfaces of twinned GaAs NWs act as effective CR centers. The calculated SRV quantitatively explains recent experimental observations. Such atomistic understanding lays a foundation for the rational design of GaAs NW-based devices.

ACKNOWLEDGMENTS

This work was supported by the U.S. Department of Energy, Office of Science, Office of Basic Energy Sciences under Award No. DE-SC0001013 as part of the Center for Energy Nanoscience, an Energy Frontier Research Center. Simulations were performed at the Center for High Performance Computing and Communications of the University of Southern California.

- ¹J. Wallentin, N. Anttu, D. Asoli, M. Huffman, I. Aberg, M. H. Magnusson, G. Siefert, P. Fuss-Kailuweit, F. Dimroth, B. Witzigmann, H. Q. Xu, L. Samuelson, K. Deppert, and M. T. Borgstrom, *Science* **339**(6123), 1057–1060 (2013).
- ²J. A. Czaban, D. A. Thompson, and R. R. LaPierre, *Nano Lett.* **9**(1), 148–154 (2009).
- ³G. Mariani, A. C. Scofield, C. H. Hung, and D. L. Huffaker, *Nat. Commun.* **4**, 1497 (2013).
- ⁴M. Yao, N. Huang, S. Cong, C.-Y. Chi, M. A. Seyedi, Y.-T. Lin, Y. Cao, M. L. Povinelli, P. D. Dapkus, and C. Zhou, *Nano Lett.* **14**(6), 3293–3303 (2014).
- ⁵H. J. Joyce, C. J. Docherty, Q. Gao, H. H. Tan, C. Jagadish, J. Lloyd-Hughes, L. M. Herz, and M. B. Johnston, *Nanotechnology* **24**(21), 214006 (2013).
- ⁶Q. H. Xiong, J. Wang, and P. C. Eklund, *Nano Lett.* **6**(12), 2736–2742 (2006).
- ⁷R. E. Algra, M. A. Verheijen, M. T. Borgstrom, L. F. Feiner, G. Immink, W. J. P. van Enkevort, E. Vlieg, and E. P. A. M. Bakkers, *Nature* **456**(7220), 369–372 (2008).
- ⁸P. Caroff, K. A. Dick, J. Johansson, M. E. Messing, K. Deppert, and L. Samuelson, *Nat. Nanotechnol.* **4**(1), 50–55 (2009).
- ⁹K. Shimamura, Z. Yuan, F. Shimojo, and A. Nakano, *Appl. Phys. Lett.* **103**(2), 022105 (2013).
- ¹⁰Z. Yuan and A. Nakano, *Nano Lett.* **13**(10), 4925–4930 (2013).
- ¹¹R. Car and M. Parrinello, *Phys. Rev. Lett.* **55**(22), 2471–2474 (1985).
- ¹²M. C. Payne, M. P. Teter, D. C. Allan, T. A. Arias, and J. D. Joannopoulos, *Rev. Mod. Phys.* **64**(4), 1045–1097 (1992).
- ¹³F. Shimojo, S. Ohmura, R. K. Kalia, A. Nakano, and P. Vashishta, *Phys. Rev. Lett.* **104**(12), 126102 (2010).
- ¹⁴K. Shimamura, F. Shimojo, R. K. Kalia, A. Nakano, and P. Vashishta, *Phys. Rev. Lett.* **111**(6), 066103 (2013).
- ¹⁵K. Shimamura, F. Shimojo, R. K. Kalia, A. Nakano, K. Nomura, and P. Vashishta, *Nano Lett.* **14**(7), 4090–4096 (2014).
- ¹⁶P. Hohenberg and W. Kohn, *Phys. Rev.* **136**(3B), B864–B871 (1964).
- ¹⁷W. Kohn and L. J. Sham, *Phys. Rev.* **140**(4A), A1133–A1138 (1965).
- ¹⁸C. F. Craig, W. R. Duncan, and O. V. Prezhdo, *Phys. Rev. Lett.* **95**(16), 163001 (2005).
- ¹⁹C. P. Hu, H. Hirai, and O. Sugino, *J. Chem. Phys.* **127**(6), 064103 (2007).
- ²⁰E. Tapavicza, I. Tavernelli, and U. Rothlisberger, *Phys. Rev. Lett.* **98**(2), 023001 (2007).
- ²¹X. Zhang, Z. Li, and G. Lu, *Phys. Rev. B* **84**(23), 235208 (2011).
- ²²W. Mou, S. Ohmura, F. Shimojo, and A. Nakano, *Appl. Phys. Lett.* **100**(20), 203306 (2012).
- ²³P. E. Blochl, *Phys. Rev. B* **50**(24), 17953–17979 (1994).
- ²⁴G. Kresse and D. Joubert, *Phys. Rev. B* **59**(3), 1758–1775 (1999).
- ²⁵J. P. Perdew, K. Burke, and M. Ernzerhof, *Phys. Rev. Lett.* **77**(18), 3865–3868 (1996).
- ²⁶S. G. Louie, S. Froyen, and M. L. Cohen, *Phys. Rev. B* **26**(4), 1738–1742 (1982).
- ²⁷F. Shimojo, S. Ohmura, W. Mou, R. K. Kalia, A. Nakano, and P. Vashishta, *Comput. Phys. Commun.* **184**(1), 1–8 (2013).
- ²⁸F. Shimojo, R. K. Kalia, M. Kunaseth, A. Nakano, K. Nomura, S. Ohmura, K. Shimamura, and P. Vashishta, *J. Chem. Phys.* **140**(18), 18A529 (2014).
- ²⁹J. Ihm, A. Zunger, and M. L. Cohen, *J. Phys. C* **12**(21), 4409–4422 (1979).
- ³⁰F. Shimojo, R. K. Kalia, A. Nakano, and P. Vashishta, *Comput. Phys. Commun.* **140**(3), 303–314 (2001).
- ³¹K. Nomura, R. K. Kalia, A. Nakano, P. Vashishta, K. Shimamura, F. Shimojo, M. Kunaseth, P. C. Messina, and N. A. Romero, *Int. Conf. High Performance Comput., Networking, Storage Analysis* **14**, 661–673 (2014).
- ³²W. Gropp, E. Lusk, and A. Skjellum, *Using MPI*, 3rd ed. (MIT Press, Cambridge, MA, 2014).

- ³³M. E. Casida, in *Recent Advances in Density Functional Methods (Part I)*, edited by D. P. Chong (World Scientific, Singapore, 1995), pp. 155–192.
- ³⁴J. C. Tully, *J. Chem. Phys.* **93**(2), 1061–1071 (1990).
- ³⁵J. R. Schmidt, P. V. Parandekar, and J. C. Tully, *J. Chem. Phys.* **129**(4), 044104 (2008).
- ³⁶O. V. Prezhdo, *J. Chem. Phys.* **111**(18), 8366–8377 (1999).
- ³⁷A. W. Jasper, S. N. Stechmann, and D. G. Truhlar, *J. Chem. Phys.* **116**(13), 5424–5431 (2002).
- ³⁸H. M. Jaeger, S. Fischer, and O. V. Prezhdo, *J. Chem. Phys.* **137**(22), 22A545 (2012).
- ³⁹C.-Y. Chi, C.-C. Chang, S. Hu, T.-W. Yeh, S. B. Cronin, and P. D. Dapkus, *Nano Lett.* **13**(6), 2506–2515 (2013).
- ⁴⁰Z. Yuan, K. Shimamura, F. Shimojo, and A. Nakano, *J. Appl. Phys.* **114**(7), 074316 (2013).
- ⁴¹G. Priante, J. C. Harmand, G. Patriarche, and F. Glas, *Phys. Rev. B* **89**(24), 241301(R) (2014).
- ⁴²N. Moll, A. Kley, E. Pehlke, and M. Scheffler, *Phys. Rev. B* **54**(12), 8844–8855 (1996).
- ⁴³X. J. Zhu, S. B. Zhang, S. G. Louie, and M. L. Cohen, *Phys. Rev. Lett.* **63**(19), 2112–2115 (1989).
- ⁴⁴Z. Yuan, K. Nomura, and A. Nakano, *Appl. Phys. Lett.* **100**(16), 163103 (2012).
- ⁴⁵Z. Yuan, K. Nomura, and A. Nakano, *Appl. Phys. Lett.* **100**(15), 153116 (2012).
- ⁴⁶W. Mou, S. Ohmura, S. Hattori, K. Nomura, F. Shimojo, and A. Nakano, *J. Chem. Phys.* **136**(18), 184705 (2012).
- ⁴⁷S. Hattori, W. Mou, P. Rajak, F. Shimojo, and A. Nakano, *Appl. Phys. Lett.* **102**(9), 093302 (2013).
- ⁴⁸W. Mou, S. Hattori, P. Rajak, F. Shimojo, and A. Nakano, *Appl. Phys. Lett.* **102**(17), 173301 (2013).
- ⁴⁹T. Watanabe, K. Tatsumura, and I. Ohdomari, *Phys. Rev. Lett.* **96**(19), 196102 (2006).
- ⁵⁰S. Hirose, I. Yamashita, R. Nagumo, R. Miura, A. Suzuki, H. Tsuboi, N. Hatakeyama, A. Endou, H. Takaba, M. Kubo, and A. Miyamoto, *Jpn. J. Appl. Phys. Part 1* **50**(4), 04DP05 (2011).
- ⁵¹X. Dai, S. A. Dayeh, V. Veeramuthu, A. Larrue, J. Wang, H. B. Su, and C. Soci, *Nano Lett.* **11**(11), 4947–4952 (2011).
- ⁵²K. Tomioka, M. Yoshimura, and T. Fukui, *Nature* **488**(7410), 189–192 (2012).
- ⁵³F. Shimojo, A. Nakano, R. K. Kalia, and P. Vashishta, *Phys. Rev. E* **77**(6), 066103 (2008).